Quantitative Magnetic Resonance Imaging Assessment of the Quadriceps Changes during an Extreme Mountain Ultramarathon

HOAI-THU NGUYEN[1], THOMAS GRENIER[2], BENJAMIN LEPORQ[2], CAROLINE LE GOFF[3], BENJAMIN GILLES[4], SYLVAIN GRANGE[1,5], RÉMI GRANGE[1,5], GRÉGOIRE P. MILLET[6], OLIVIER BEUF[2], PIERRE CROISILLE[1,5], and MAGALIE VIALLON[1,5]

[1]Univ-Lyon, UJM-Saint-Etienne, INSA-Lyon, Université Claude Bernard Lyon 1, CNRS, Inserm, Saint-Etienne, FRANCE; [2]Univ Lyon, INSA-Lyon, Université Claude Bernard Lyon 1, UJM-Saint Etienne, CNRS, Inserm, Villeurbanne, FRANCE; [3]Department of Clinical Chemistry, University of Liège, CHU Sart-Tilman, Liège, BELGIUM; [4]LIRMM, Université Montpellier, CNRS, Montpellier, FRANCE; [5]Department of Radiology, Centre Hospitalier Universitaire de Saint Etienne, Université de Saint Etienne, Saint Etienne, FRANCE; and [6]Institute of Sport Sciences, University of Lausanne, Lausanne, SWITZERLAND

ABSTRACT

NGUYEN, H.-T., T. GRENIER, B. LEPORQ, C. LE GOFF, B. GILLES, S. GRANGE, R. GRANGE, G. P. MILLET, O. BEUF, P. CROISILLE, and M. VIALLON. Quantitative Magnetic Resonance Imaging Assessment of the Quadriceps Changes during an Extreme Mountain Ultramarathon. *Med. Sci. Sports Exerc.*, Vol. 53, No. 4, pp. 869–881, 2021. **Introduction/Purpose:** Extreme ultra-endurance races are growing in popularity, but their effects on skeletal muscles remain mostly unexplored. This longitudinal study explores physiological changes in mountain ultramarathon athletes' quadriceps using quantitative magnetic resonance imaging (MRI) coupled with serological biomarkers. The study aimed to monitor the longitudinal effect of the race and recovery and to identify local inflammatory and metabolic muscle responses by codetection of biological markers. **Methods:** An automatic image processing framework was designed to extract imaging-based biomarkers from quantitative MRI acquisitions of the upper legs of 20 finishers at three time points. The longitudinal effect of the race was demonstrated by analyzing the image markers with dedicated biostatistical analysis. **Results:** Our framework allows for a reliable calculation of statistical data not only inside the whole quadriceps volume but also within each individual muscle head. Local changes in MRI parameters extracted from quantitative maps were described and found to be significantly correlated with principal serological biomarkers of interest. A decrease in the PDFF after the race and a stable paramagnetic susceptibility value were found. Pairwise *post hoc* tests suggested that the recovery process differs among the muscle heads. **Conclusions:** This longitudinal study conducted during a prolonged and extreme mechanical stress showed that quantitative MRI-based markers of inflammation and metabolic response can detect local changes related to the prolonged exercise, with differentiated involvement of each head of the quadriceps muscle as expected in such eccentric load. Consistent and efficient extraction of the local biomarkers enables to highlight the interplay/interactions between blood and MRI biomarkers. This work indeed proposes an automatized analytic framework to tackle the time-consuming and mentally exhausting segmentation task of muscle heads in large multi–time-point cohorts.
Key Words: MUSCULOSKELETAL, STATISTICAL ANALYSIS, IMAGE PROCESSING, FUNCTIONAL VARIATION

Mountain ultra-endurance running consists of running/walking outdoors over a distance longer than the traditional marathon on mountain trails with significant upward and downward slopes. This sport has become increasingly popular over the last decade.

Address for correspondence: Magalie Viallon, Ph.D., Service de radiologie, CHU de Saint Etiennem Avenue Albert Raimond, 42055 Saint Etienne Cedex 2, France; E-mail: magalie.viallon@creatis.insa-lyon.fr.
Submitted for publication July 2020.
Accepted for publication September 2020.
Supplemental digital content is available for this article. Direct URL citations appear in the printed text and are provided in the HTML and PDF versions of this article on the journal's Web site (www.acsm-msse.org).

0195-9131/20/5304-0869/0
MEDICINE & SCIENCE IN SPORTS & EXERCISE®

DOI: 10.1249/MSS.0000000000002535

Because of the inherent challenge for the body, the mountain ultramarathon (MUM) is considered an outstanding model to investigate the adaptive responses to extreme load and mechanical stress (1) in skeletal muscles. Studies have been carried out to explore the effect of these prolonged cardiovascular and muscle efforts, demonstrating, for instance, multiple visceral changes with inflammatory effects (2–4) or an impairment of neuromuscular function (5). Among all muscles, the quadriceps are particularly targeted because extensive downhill running causes repeated eccentric contractions and high mechanical stress, ultimately leading to muscle damage (6,7).

Magnetic resonance imaging (MRI) is a reliable, nonirradiating and noninvasive imaging method for tissue characterization and quantitative assessment of tissue integrity through its magnetic properties. Indeed T2 MR relaxation times and its corresponding rates R2 (=1/T2) denote the characteristic time constants of the recovery back toward equilibrium of the *xy*

(transverse) components of the magnetization. After being disturbed, the MR signal source, that is, nuclear magnetization, does not spontaneously recover very fast but relies almost entirely on interactions of hydrogen nuclei with the surrounding material to reequilibrate (8). Because T2 is sensitive to low-frequency components, in tenth of ms, water molecules diffuse and sample many different environments on the cellular level within the timescale of relaxation. In many (although by no means all) situations, very rapid exchange may occur between bulk water and bound and interfacial water in biological systems. This is believed to be the origin for many T2 changes in various pathologies, such as edematous changes after insults to tissue. Changes in tissue water and protein content have been shown to affect relaxation. The measure of average water proton relaxation rate will depend on how effectively and at what rate these effects are spread through the rest of the water population. Moreover, the existence of water in separate compartments that are only slowly exchanging gives rise to more complex behavior (9). Many studies witness that edematous areas in the muscle appear bright in T2-weighted images because the T2 relaxation time becomes longer, and T2 maps show elevated quantitative values in the matching area (10,11). T2 maps have therefore been used to monitor inflammation in muscle diseases, before and after medical interventions or treatment (12–14), or to predict return to play (15). T2* is the "effective" T2 resulting from inhomogeneities in the main magnetic field or susceptibility-induced field distortions produced in the tissue, related to the presence of chemical or paramagnetic substances such as fat or hemorrhage (16). However, the first step in decoding the various effects of prolonged exercise stress on the body using quantitative MRI (qMRI) markers is to develop systematic and comprehensive noninvasive exploration strategies to consistently extract the biomarkers reflecting the physiological consequences of such challenges.

From that perspective, MRI seems to be a unique imaging modality for extracting anatomical and structural features of muscle tissue (17,18). Recently, quantitative imaging methods such as chemical shift-encoded MRI (19,20) and MR relaxometry mapping (21,22) have allowed users to understand chemical alterations noninvasively at the imaged pixel size.

Several postprocessing methods need to be sequentially applied to extract a quantitative index from MRI data. These methods include the segmentation of muscle heads on multiple large three-dimensional (3D) images, the extraction of image features in each area of interest, and statistical analysis. Each of these steps is an area of research in its own right. Although various alternatives have been proposed to target each of these challenges (17,18), they are rarely applied to cohorts or longitudinal studies.

The aims of the study were to quantify the response of the quadriceps muscle to a MUM's extreme loading conditions with qMRI and to monitor the longitudinal effect of race and recovery. To do so, we propose an automatized and integrated analysis pipeline that enables the extraction of local quantitative imaging markers. Hence, the relation of these new markers with standard blood biomarkers was investigated to provide further insight into the local inflammatory and metabolic muscle responses.

MATERIALS AND METHODS

Subjects and Experimental Study Design

We performed a longitudinal study on the athletes who participated in the "Tor des Géants" MUM in 2014, including three MRI sessions carried out just before the start and, for those who finished the race, immediately upon arrival and after 48 h of recovery. Biological samples were also drawn at four time points, with an additional sample obtained at half-race. The flowchart of the study is shown in Figure 1.

This study was approved by the local ethical committee (Aosta Valley, Azienda USL 101/946), and the experimental plan was conducted in accordance with the Helsinki Declaration (2001). Subjects were recruited through mailing and public announcements to registered runners by race organizers. Exclusion criteria were smoking, substance abuse, regular intake of medications, medical or psychiatric illness, and any contraindication to MRI (e.g., claustrophobia and nonremovable metal devices) or abnormalities detected upon laboratory screening. There were 50 experienced runners who volunteered and provided informed written consent to participate in this study.

The Tor des Géants is a 330-km-long ultradistance trail running, with considerable positive/negative elevation changes (+24,000 m) in the Valley of Aosta (Italy). It is considered one of the most difficult mountain marathon races in the world because the ultra-endurance activity is associated with high-altitude exposure and sleep deprivation. The altitude along the course ranges between 322 and 3300 m, with 25 mountain passes over 2000 m. The maximum time allowed to complete the race is 150 h, and in 2014, the best performance was 71 h 49 min among 740 starters and 446 (60%) finishers (http://www.tordesgeants.it/).

The present experimental design was thus a longitudinal study with repeated assessments at four checkpoints:

- The first point (prerace: Pre) was at the start location. The data collection was performed within 4 d before the race and consisted of MRI acquisition and biological sampling.
- The second point was located halfway through the race (middle: Mid). Only biological sampling was performed.
- The third one was at the arrival of the race (arrival: Post): athletes who finished the race were transported by car to the laboratory and were evaluated (MRI and biological sampling) within 1 h after finishing the race.
- The last point (recovery: Post+3) was 48–72 h after arrival time. Both MRI and biological sampling were acquired.

MRI Acquisitions

At Pre, Post, and Post+3 time points, MRI acquisitions were performed on site using a mobile 1.5-T MR scanner system

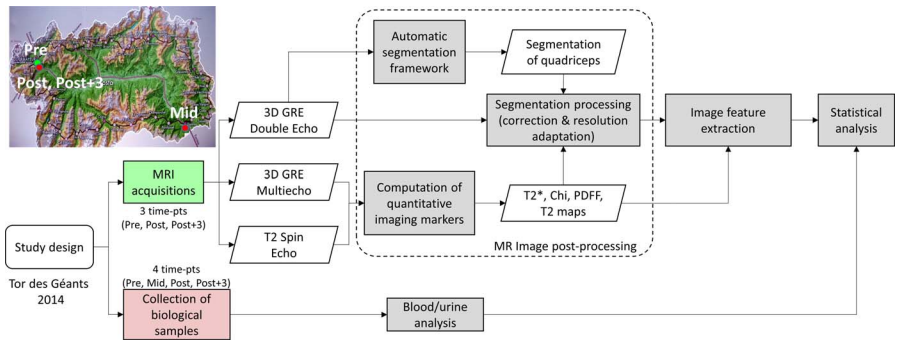

FIGURE 1—Flowchart summarizing the main steps of our study. MRI was performed at three time points: before (Pre) and, for participants who finished the race, immediately after (Post) and ~48–72 h after the race (Post+3). Meanwhile, biological sampling was performed at four time points (an additional sample was performed at half-race (Mid)).

(MAGNETOM Avanto; Siemens Healthcare, Erlangen, Germany, located within a truck from Alliance Medical, England). A standard coil configuration was used: a flexible four-channel array surface coil, combined with four elements of the spine coil embedded in the bed, resulting in an eight-channel coil in total.

Three MRI acquisitions of the legs were sequentially performed:

- A 3D isotropic gradient dual-echo sequence was used. The coronal acquisition included the entire upper leg (from the tibial tuberosity to the anterior superior iliac spine). The reconstruction of the water and fat images from the acquired dual-echo data sets was performed inline (Syngo software; Siemens Healthcare, Erlangen, Germany) using a Dixon approach enabling four 3D isotropic in-phase, out-phase, fat and water coronal images to be calculated inline on the MR scanner, hereafter denoted water (W), fat (F), in-phase (IN), and out-phase (OUT) images, respectively.
- A 3D spoiled gradient echo sequence (3D GRE) was used for simultaneous estimation of proton density fat fraction (PDFF), T2*, and internal magnetic susceptibility (χ) quantification. Eight echoes were acquired in the transverse plane with a flyback readout gradient (first echo, 1.58 ms; echo spacing, 2.52 ms). TR and flip angle were adjusted to minimize the T1-related bias. Phase and magnitude images were systematically reconstructed. Prescription of localization was performed using anatomic images from an isotropic 3D gradient echo acquisition. For standardization purposes, the central partition in the *z*-direction was planned at a 15-cm distance from the upper part of the patella using the sagittal multiplanar reconstruction of the first acquired 3D gradient isotropic sequence.
- A two-dimensional multiecho T2-weighted spin-echo sequence (meSE), with 16 echo times ranging from 10 to 178 ms, with its central slice was also planned at the same location as previously described.

Each individual sequence was individually optimized. Anatomical regions explored by each technique are summarized in Figure 2A, and the main MR parameters are listed in Supplemental Digital Content 1, MR imaging acquisition parameters, http://links.lww.com/MSS/C174.

MR Image Postprocessing

PDFF, χ, and T2* were calculated from 3D GRE acquisition using the reconstruction method described in Refs. (19–22), which encompassed two main steps: fat–water separation (provided parametric T2* and PDFF maps) and magnetic susceptibility quantification. Meanwhile, T2 parametric maps were calculated from the meSE sequences.

An automatic segmentation based on external force–driven deformable registration was performed on the T1-weighted images (24) to obtain the quadriceps heads of interest.

Briefly, dedicated in-house postprocessing pipelines were required 1) to simultaneously compute the main parametric maps (fat fraction − PDFF, internal magnetic susceptibility (χ) and T_2* from the 3D GRE sequence, T2 parametric map from the meSE sequence) and 2) to correct the results of the automatic muscle segmentation and to adjust their resolutions to different image sequences (Fig. 2). These steps allowed us to extract metrics from the four parametric maps: PDFF, χ, T2*, and T2. All details about parametric map reconstruction and muscle segmentation are provided in Supplemental Digital Content 2, quantitative maps computation, http://links.lww.com/MSS/C175, and Supplemental Digital Content 3, muscle segmentation procedure, http://links.lww.com/MSS/C176.

Biological Sampling and Analysis

Blood and urinary samples were collected at each of the four sessions (Pre, Mid, Post, Post+3) within 10 min after arrival at each key point. Blood samples were drawn from an antecubital vein into a dry, heparinized, or EDTA tube according to the analysis to be performed and immediately centrifuged. Because it was not possible to carry out all the investigations on the same day by point-of-care technologies, plasma and serum were frozen at −80°C within 20 min after blood collection for later analysis of muscle injury markers and biochemical variables. The hematology parameters (hemoglobin, red blood cells, white blood cells) were directly analyzed by a pocH-100i™ automated hematology analyzer (Sysmex, Villepinte,

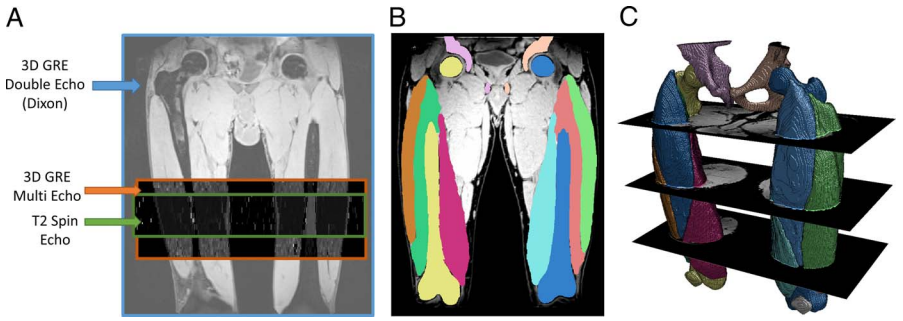

FIGURE 2—MRI input sequences superposed on the isotropic water image (A), and the coronal view of the automatic segmentation displayed with the isotropic water image as a background (B) and its 3D volume (C) rendered with 3DSlicer (23).

France). Cobas 8000 (RocheDiagnostics, Manheim, Germany) was used to perform serial determinations for C-reactive protein, urinary creatinine, creatinine, calcium, chlorine, potassium, sodium, and cholesterol. The osmolality and urinary osmolality were measured on an Arkray Osmo Station OM-6050 (Menarini, Florence, Italy).

All blood biomarkers analyzed in this study are listed in Supplemental Digital Content 4, complete list of 58 biological markers analyzed in the study, http://links.lww.com/MSS/C177.

Statistical Analysis

Missing values in biological data sets were estimated (Supplemental Digital Contents 5, biological data preprocessing for missing data, http://links.lww.com/MSS/C178) to use paired statistical tests and for subsequent correlation analysis between MRI and biological markers. The significance level was set at $P < 0.05$ for all statistical tests.

Longitudinal statistical analysis. For the qMRI longitudinal data, we used a statistical analysis of repeated measures with adaptation to the data normality, as the normal distribution could not be assumed. For each qMRI-calculated index of each of the nine muscle volumes (four quadriceps muscle heads per leg and the total quadriceps volume), we tested the normality of the data at three time points with the Shapiro–Wilk test. For the global effect test, one-way ANOVA designed for repeated measures was conducted for all data normally distributed at all the time points; otherwise, the Friedman test was used.

While performing ANOVA, the sphericity of the data was verified by using Mauchly's test. If the sphericity assumption was violated, the Greenhouse–Geisser correction method was used on the P value of ANOVA. After the global effect test, a *post hoc* test was performed to compare each pair of time points. The type of *post hoc* test depended on the normality of differences between two time points: dependent t-test for normally distributed differences and Wilcoxon signed rank test, otherwise. The obtained P values were adjusted with the Bonferroni adjustment method for multiple comparisons.

A similar strategy was applied to the biological marker data with 58 variables at four time points. Relative variations of a biomarker X at each time point ($\mathrm{RV}(X_n)$, $n \in \{\mathrm{Mid}, \mathrm{Post}, \mathrm{Post}+3\}$) compared with time point Pre were also computed with:

$$\mathrm{RV}(X_n) = \frac{\overline{X_n} - \overline{X_{\mathrm{Pre}}}}{\overline{X_{\mathrm{Pre}}}} \times 100\%$$

where $\overline{X_n}$ is the average value of biomarker X at time point n.

Associations between image markers and biological markers. The potential associations between image markers and biological markers were evaluated by calculating the repeated-measures correlation coefficient (25) between each image marker and each biological marker.

RESULTS

MR markers: parametric mapping analysis. Of the 50 athletes who were included in the study, 31 finishers completed the race (62%) in an average time of 124 ± 13 h. Among them, only those with quadriceps muscle MRI data sets available at all the time points ($n = 24$) and with quantitative maps free of artifacts at all three time points were retained for final analysis ($n = 20$). Artifacts leading to data exclusions were mostly motion-related. They were specifically due to uncontrolled motion of the legs typically observed immediately after long races potentially combined with those related to sudden sleep attacks during MR acquisitions. Demographic data and global qMRI metrics collected at each time point are reported in Supplemental Digital Content 6, demographic data and qMRI metrics of the subject population, http://links.lww.com/MSS/C179.

The first step was to explore differences among all quadriceps muscle heads. Figure 3 shows a matrix of the t-test results when comparing qMRI metrics (χ, PDFF, T2, T2*) between all muscle heads at the three MR acquisition time points (Pre, Post, Post+3). When focusing only on right/left differences of the corresponding muscle heads, χ, T2*, and PDFF showed similar tendency. At the same time, there was no significant difference between right and left muscle heads for χ and T2* at any time point, and PDFF exhibited a significant difference between vastus lateralis (VL) heads only at a single time point (Post+3). On the other hand, the T2 metric showed a different pattern with a significant difference between the rectus femoris (RF) heads of the two legs at the three time points (Pre, Post, Post+3) and a significant difference between the left and right vastus medialis (VM) at time point Pre. Different muscle

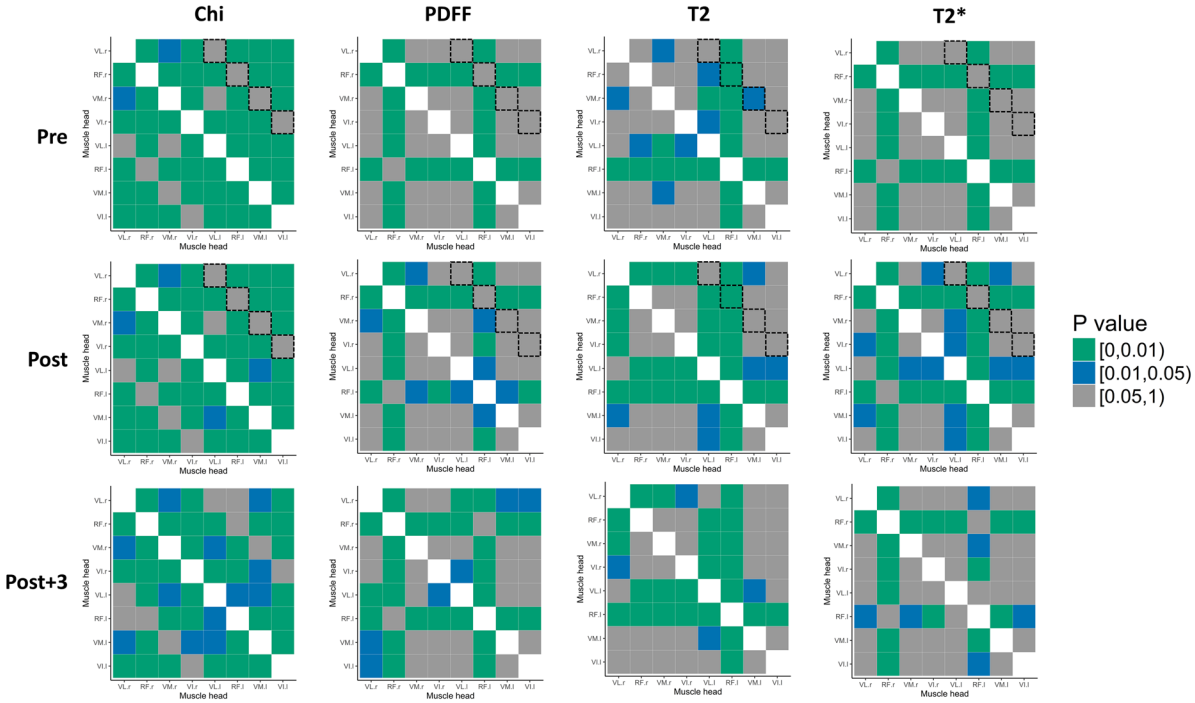

FIGURE 3—*t*-Test matrix with color-coded *P* values for multiple comparisons of qMRI metrics (χ, PDFF, T2, T2*) between muscle heads at all three acquisition time points (Pre, Post, Post+3). VL, vastus lateralis; RF, rectus femoris; VM, vastus medialis; VI, vastus intermedius; r, right; l, left. For easy viewing, dotted diagonals highlight interleg (right/left) comparisons of the same muscle heads at each time point, whereas all other boxes are intraleg and/or interhead comparisons.

heads also had different qMRI values, especially the RF, which showed significant differences compared with all the other muscle heads most of the time. These results highlight the need to consider individual muscle behavior separately and that pooling quadriceps muscle heads may result in a loss of information.

When analyzing temporal changes on the repeated measures of qMRI metrics, we observed a significant time effect (i.e., race effect) on T2* and T2 mean values. This is shown in Figures 4 and 5 with typical source images (see also Supplemental Digital Content 6, demographic data and qMRI metrics of the subject population, http://links.lww.com/MSS/C179, for summary values and Supplemental Digital Content 7, specific longitudinal T2* analysis, for a local analysis of right VI in T2* for an example subject, http://links.lww.com/MSS/C180). Both T2* and T2 were significantly longer at arrival for most of the muscle heads. They significantly decreased after recovery for the VM and the vastus intermedius (VI) while not returning to baseline values at that time of measurement.

PDFF and χ showed only a small time effect (Figs. 6, 7). Pooling all muscles, PDFF had a tendency to decrease after the race (2.88 ± 0.53) compared with baseline (3.16 ± 0.45), whereas it increased to higher values than baseline (3.17 ± 0.46) after 48 h of recovery. When considering each muscle, the time effect reached significance for VI, right VM, and left VL muscle heads (Fig. 6). Despite a similar trend as the PDFF, time-effect changes in χ did not reach significance for most muscle heads, except for left VL and left VM (L).

When focusing on T2* and T2 findings, the vastus group exhibited stronger variations than did the RF muscle group. The VM and VI had larger changes than did the VL or the average of all muscles. T2* values seemed to be less sensitive to muscle changes than T2, as illustrated in Figure 3, but most of the statistical tests were significant except for some muscle heads on both legs between time points Post and Post+3.

Biological marker analysis. The longitudinal variations in biological markers throughout the race are shown in Supplemental Digital Content 8, values of urinary and blood biomarkers at 4 time points, http://links.lww.com/MSS/C181. As main blood biomarkers of muscle damage, serum creatine kinase (CK) and myoglobin levels peaked at +6598% and +4159% at Mid, whereas serum lactate dehydrogenase (LDH) levels peaked at +240% at Post and were elevated at Mid at +197% (all *P* values of *post hoc* test against Pre are less than 0.01; Fig. 8). For most of the biomarkers, the biomarker values at Pre were significantly different from those at the other time points (Mid, Post, Post+3), whereas the difference between Mid and Post was nonsignificant.

Correlation between qMRI features and main blood biomarkers. We presented our results with a heatmap produced within R software (Supplemental Digital Content 9, correlation between biological markers and image features extracted from quadriceps muscles in each qMRI quantitative map, http://links.lww.com/MSS/C182). An interactive version of this heatmap can be found online (http://amp.pharm.mssm.edu/clustergrammer/viz_sim_mats/5bed953490fbf7585f5680c2/Correlation_Mean.txt), thanks to Clustergrammer (26). Significant

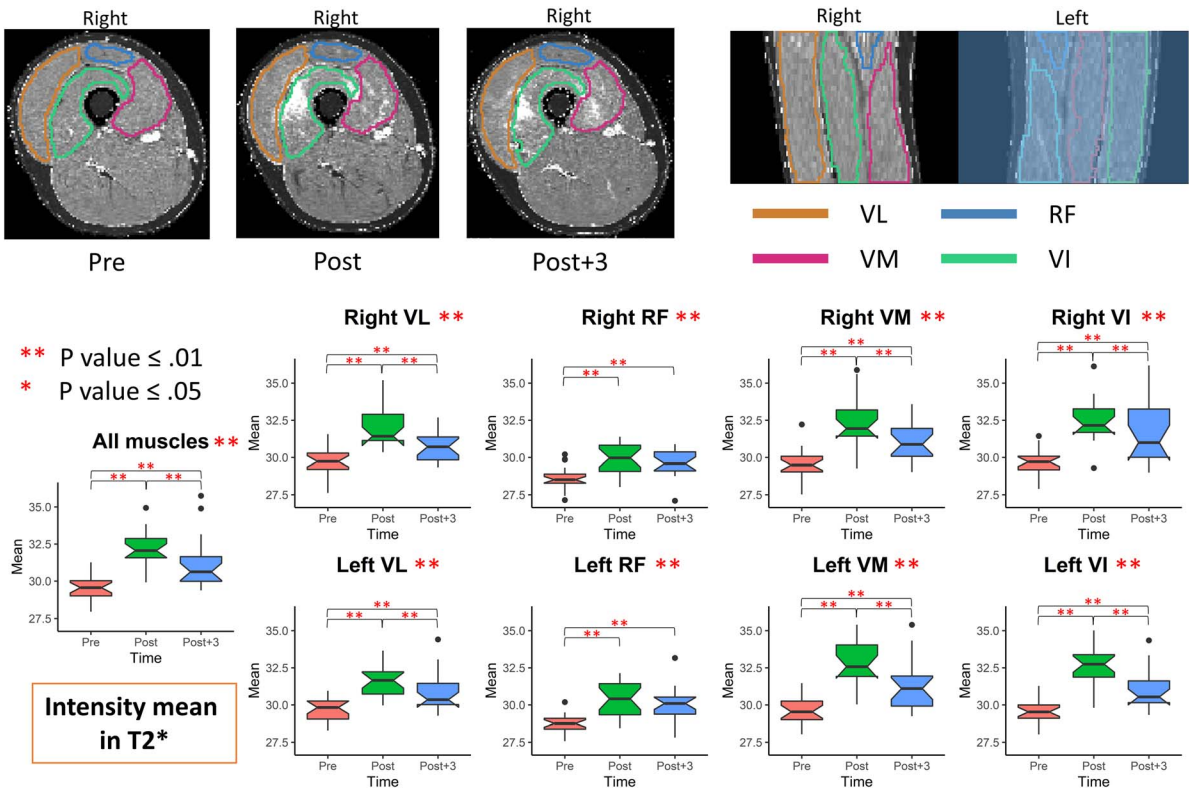

FIGURE 4—Variation of T2* mean in the individual muscle heads of all finishers with an example of T2* maps at the three MR acquisition time points relative to the race of the same subject. A *P* value less than 0.05 indicates a significant change between two time points. VL, vastus lateralis; RF, rectus femoris; VM, vastus medialis; VI, vastus intermedius.

correlations between qMRI features and biological markers were found:

- The T2 mean extracted from the whole quadriceps showed a significant time effect at all time points of the race and a relatively strong correlation with blood/urine biomarkers such as myoglobin (0.69), CK (0.78), and LDH (0.72). At the level of individual muscles, the correlation coefficient is higher for VI and VM muscles.
- T2* exhibited similar results but with lower correlation coefficients: 0.54 for myoglobin, 0.57 for CK, and 0.61 for LDH.
- Meanwhile, neither the mean global PDFF nor χ showed any significant correlation coefficients with biological markers in this study.

DISCUSSION

Although ultraloading events such as MUMs are recognized to endanger the musculoskeletal system, little is known about the exact consequences of the acute biomechanical burden on musculoskeletal tissues. Although Lucas et al. (27) recommend the use of MRI as the method of choice for studying endurance-related damage, to date, there has been only one longitudinal observational field cohort study focusing primarily on changes in overall body composition (28) or morphological tissue damage (29).

The challenge and novelty of this work are twofold: 1) first, to provide a technological approach specifically developed enabling the extraction of qMRI parameters for longitudinal skeletal muscle studies, 2) then, to demonstrate that qMRI brings unique insights into the response of quadriceps muscle exposed to prolonged mechanical stress of a 330-km ultra-endurance event.

To do so, we built a standardizing and automatic analysis pipeline that segments, calculates, and extracts all qMRI markers in each quadriceps muscle's head that can be robustly propagated to the different follow-up time points, thus enabling longitudinal monitoring.

Beyond the scope of this work, our first contribution is to empower a comprehensive and multiparametric quantification of MRI biomarkers in thigh skeletal muscle, including T2 and T2* relaxation times, together with fat content (PDFF), and internal magnetic susceptibility χ. Second, the analysis framework enabled the analysis of each quadriceps muscle head over different time points (Supplemental Digital Content 6, demographic data and qMRI metrics of the subject population, http://links.lww.com/MSS/C179, and Figs. 4–7).

Our main findings are that the cumulative biomechanical stress of a 330-km MUM onto quadriceps muscles translated in our subjects to a clear inflammatory burden with an increase in T2 and T2* relaxation times. On the other hand, muscular metabolic and energy storage status probed fat content (PDFF) remained relatively stable with a small decrease in PDFF,

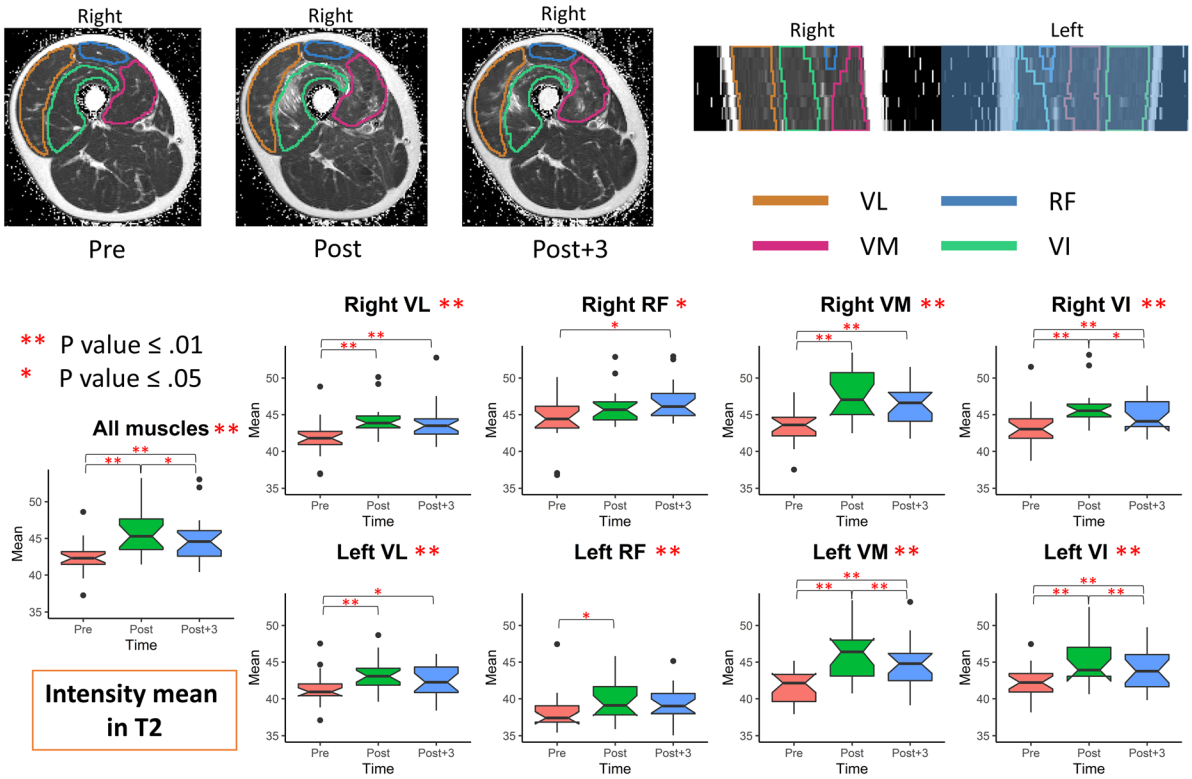

FIGURE 5—Variation of T2 mean in the individual muscle heads of all finishers with an example of T2 maps at the three MR acquisition time points relative to the race of the same subject. A *P* value less than 0.05 indicates a significant change between two time points. VL, vastus lateralis; RF, rectus femoris; VM, vastus medialis; VI, vastus intermedius.

contrasting with the high energy expenditure that mainly relies on lipids. Hereinafter is a detailed discussion of each qMRI finding.

T2 and T2* changes: MR markers of the muscular inflammatory burden. T2 and T2* changes (Supplemental Digital Content 6, demographic data and qMRI metrics of the subject population, http://links.lww.com/MSS/C179, and Figs. 4, 5) are an expression of the well-known sensitivity of qMRI T2 and T2* relaxation time parameters to overall water content variations and water redistribution between intracellular and extracellular spaces (18,22,30–33). Our findings confirm previous studies that reported with other approaches a significant inflammatory response after MUM (5,34), mainly related to repetitive eccentric muscle contractions resulting in microscopic muscle damage and subsequent edema (5,6,35). In our study, T2 and T2* remained elevated even after a few days of recovery, suggesting that 48–72 h is not sufficient for a full recovery in most subjects and confirming previous findings by Robach et al. (36).

Relaxometry changes demonstrated at the muscular level were corroborated by a large increase in skeletal myocyte injury–related biomarkers (CK, myoglobin, and LDH) that was also measured in our subjects. These blood biomarkers are known to witness microlesions and early signs of cellular inflammatory processes preceding water redistribution from intracellular to extracellular compartments and have also been shown to reflect the extent of cellular damage (34,37). Among the other findings in the biological profiles, white blood cell activation, particularly neutrophil activation, is known to trigger cellular and humoral inflammatory responses (38) characterized by elevated C-reactive protein levels and the presence of leucocytes in the extracellular and extravascular spaces in response to long-term exercise (34,39). The intrinsic strength of MR imaging relies on its capacity to precisely reveal the local changes, whereas the evident correlation of quantified T2 and T2* parameters with biological markers most likely could reflect a difference in the temporal response of the compared biomarkers. If the tendency were similar, the amplitude of the correlation could only be due to a difference in the temporal occurrence of the inflammation signature at the blood and tissue level, hence also during the tissue recovery process.

The development of peripheral and muscular edema together with a total body water increase has been reported in the context of ultramarathon running (28), with a 6% increase in total body water after a 1200-km run over 17 consecutive days and an increase in total body water associated with tissue edema (40). Our measures of the total quadriceps muscle volume (excluding superficial tissues) illustrated the same trend but with a small increase in quadriceps muscle volume (+3.3% at the end of the race and +3.4% after 48- to 72-h recovery relative to baseline; Supplemental Digital Content 6, demographic data and qMRI metrics of the subject population, http://links.lww.com/MSS/C179: number of voxels from the 3D GRE sequence, expressing muscle volume). This observation suggests that among the potential mechanisms involved, the T2 and T2* changes

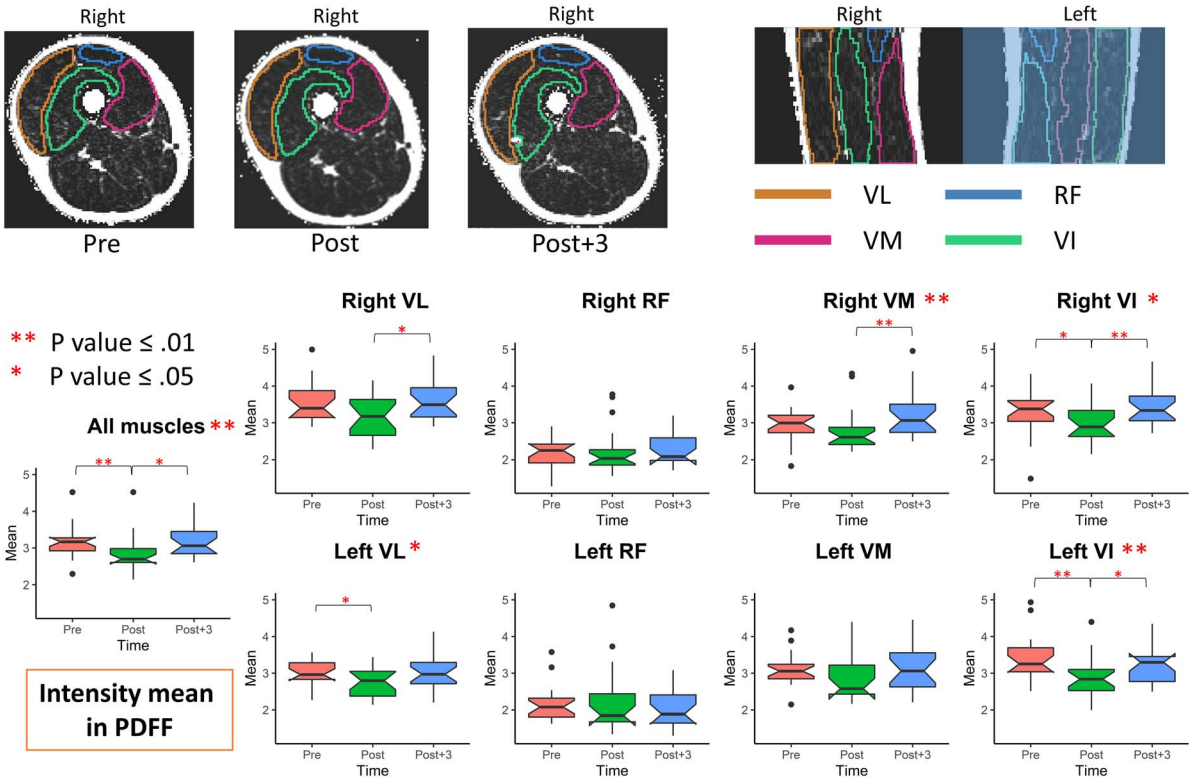

FIGURE 6—Variation of PDFF mean in the individual muscle heads of all finishers with an example of PDFF maps at the three acquisition time points relative to the race of the same subject. A *P* value less than 0.05 indicates significant changes between two time points. VL, vastus lateralis; RF, rectus femoris, VM; vastus medialis; VI, vastus intermedius.

are more likely related to water redistribution than to a net muscular tissue water content increase.

An interesting finding is the observable difference in T2 and T2* response among the different quadriceps muscle heads. Indeed, although the VI and VL exhibited both higher T2 and T2* increases, the RF showed almost no variations. These findings confirm previous studies exploring MUM and long-distance running adaptation strategies. For instance, uphill running requires considerably greater activation of the vastus group and less activation of the RF than horizontal running (41). Ultrarunners are also known to modify their running pattern by increasing their stride frequency and by reducing the vertical oscillations to minimize the load and the associated pain occurring in lower limbs mainly during the eccentric phases (42). Impact forces when running downhill can be moderated by increasing knee flexion at initial contact and reducing stride length (43). This shock attenuation strategy is also associated with a less pronounced heel strike and a forward leaning trunk. Altogether, these protective mechanical adaptations are likely to be specific to MUM and to differentially affect the quadriceps muscles, inducing less stimulation of the RF compared with the vastus muscles, which is clearly illustrated here.

From a mechanistic point of view, T2 and T2* MR relaxation measures are well established and sensitive markers of exercise response. For instance, Le Rumeur et al. (33) have shown that T2 relaxation times can detect different effects of dynamic exercise in trained and untrained subjects and that there was a correlation between T2 increase and work intensity in healthy volunteers. Beyond the observed mean variations already discussed, individual variations observed in T2 and T2* values (Fig. 4 for T2* and Fig. 5 for T2) along such long-distance running are also probably determined by a complex system of regulatory mechanisms including individual response to inflammatory processes at each compartment level, and the intrinsic differences between T2 and T2* mechanisms can probably provide further insights. Indeed, T2* mapping differentiates from T2 mapping by its ability to characterize the relaxation of the transverse magnetization that is influenced by macroscopic (inhomogeneities of the magnetic field) and mesoscopic (structure of the tissue) magnetic field inhomogeneities (44–48). For example, reduced T2* values have already shown the potential to describe structural alterations suggestive of ischemic alterations, collagen areas or hemorrhage, for instance, in myocardium and extracardiac tissues (49,50). According to this, histopathologic substrates of T2* and a correlation of T2* to flow analyses have been demonstrated (45–48,51). Recently, reduced T2* values have been described in a group of hypertrophic cardiomyopathy patients potentially triggered through relative ischemia (52). In our case, explanation for the observed increased T2* values could be related to increased perfusion and/or local variation of oxymyoglobin and oxyhemoglobin as oxygen suppliers are increased while deoxymyoglobin is decreased. Note also that increased T2*

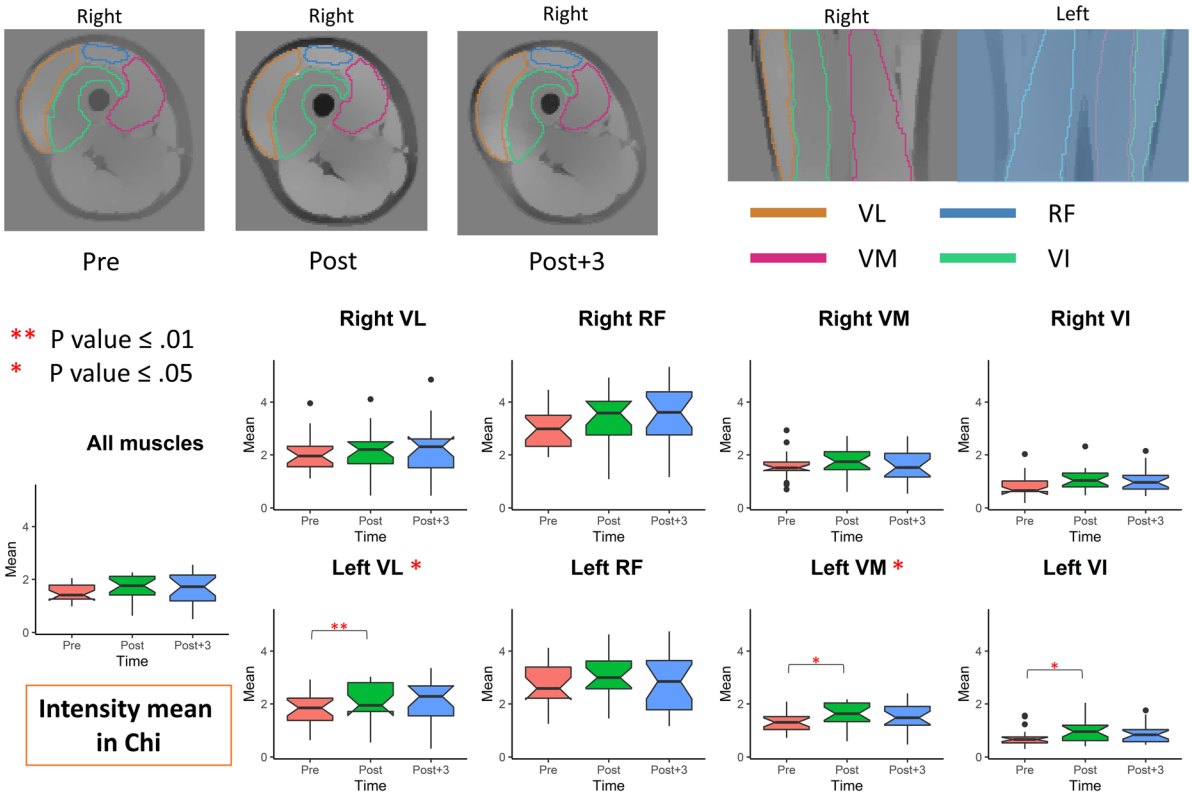

FIGURE 7—Variation of χ mean in the individual muscle heads of all finishers with an example of χ maps at the three acquisition time points relative to the race of the same subject. A *P* value less than 0.05 indicates a significant change between two time points. VL, vastus lateralis, RF; rectus femoris; VM, vastus medialis; VI, vastus intermedius.

contrast will be associated with oxygenated proteins, whereas deoxygenated proteins that are paramagnetic would reduce local T2* values.

Contrary to T2*, T2 in muscle is known to have three components: ~18% of the signal had a very short T2 (10 ms), 67% of the signal had an intermediate T2 (~40 ms), and the remaining 15% of the signal had a long T2 (~170 ms) (53). The short T2 component is the water bound to macromolecules, and the intermediate and long components represent intracellular and interstitial water, respectively. The literature also clearly describes a unidirectional flow of water from the "innermost" to "outermost" of three compartments connected in series (intracellularly bound water → free intracellular water → interstitial water → lymphatic vessels). The latter three are subject to considerable variations as a result of normal physiological changes in the muscle. In our study and because of MR acquisition technical constraints, the relaxation in the tissue could be modeled only as a unique compartment. Using a single exponential to describe T2 decay in muscle limits our understanding of the exact contributions of different physiological and biochemical responses to exercise.

PDFF and muscular lipid storage. Our study analyzed noninvasively the local variations in fat content in skeletal muscles during an ultra-endurance running event. With PDFF mapping, MRI is indeed the only noninvasive method that can enable simultaneous, reliable, and repeatable fat fraction estimates within each muscle's heads not achievable by alternative methods such as MR spectroscopy (54).

Overall, muscular fat content showed a small decrease at the end of the race, but the changes were not statistically significant except in the most solicited muscle heads (vastus group; Fig. 3).

Exploring muscular fat content variations during an MUM was of special interest because lipids are the main source of energy in low- to moderate-intensity exercises, such as long-distance events. In addition, the highest rates of fat oxidation

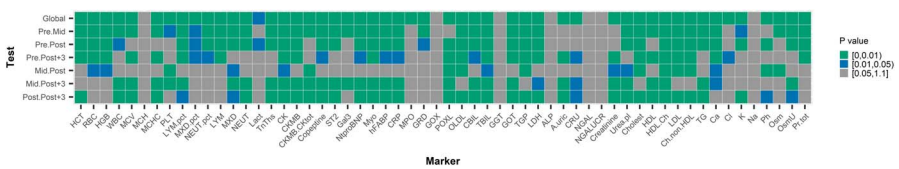

FIGURE 8—*P* values of statistical tests in our longitudinal analysis on the blood and urinary biomarker data sets. A *P* value less than 0.05 indicates a significant change between two time points.

are observed to be less than 65% in endurance athletes (55,56), which is in accordance with what has been measured on the Tor des Géants MUM by Maufrais et al. (57), who reported an average exercise intensity less than 50% of maximal oxygen uptake ($\dot{V}O_{2max}$).

Muscle fat content is mainly represented by small quantities of triglycerides (TG) that are present as lipid droplets located between or inside muscle fibers (intramyocellular TG, or IMTG), whereas most fat storage is mainly located in subcutaneous and deep visceral adipose tissue (58). There is now clear evidence that the IMTG pool acts as a buffer-regulating fatty acid (FA) flux in skeletal muscle both during exercise to maintain intracellular FA (metabolite) concentrations and in conditions of increased plasma FA provision (59,60). Our findings are in line with other studies that also reported no or minimal reduction of IMTG using biopsies before and after exercise (61–63). Using 1H-MR spectroscopy, other authors reported larger changes with an ~25% IMTG decrease after 2–3 h of exhaustive running at 50%–65% $\dot{V}O_{2max}$ (64,65). Both approaches have been challenged as suffering from intrinsic bias: the direct biopsy approach is subject to between-biopsy variability (reported up to 23%), whereas 1H-MR spectroscopy modeling accuracy may be biased by water content changes and assumptions of FA compositions in IMTG (66). All existing studies have explored fat content changes in short-duration (up to 3 h) and high-intensity (up to 80% $\dot{V}O_{2max}$) exercises that profoundly differ from MUM, which intrinsically limits comparison.

Although the IMTG pool seemed to behave as a buffer to facilitate mitochondrial oxidation and skeletal muscle energy supply, our blood lipid profiles showed a marked reduction in circulating TG and LDL because the lipoprotein lipase released by endothelial cells during exercise has been shown to increase FA availability (67). At the same time, we observed an increase in HDL cholesterol that coincides with significant increases in lipoprotein lipase activity (68) as already reported in long-distance exercise (69).

Paramagnetic susceptibility χ. Magnetic susceptibility χ is a physical property that describes the response of a medium being placed within a magnetic field (70). A positive susceptibility value characterizes a paramagnetic medium (O_2, salts) with a magnetic field increase, whereas most biological tissues, including water and fat, are diamagnetic, with negative values inducing a local decrease of the initial magnetic field.

All magnetic susceptibilities measured in our subjects and all time points were paramagnetic coherently with the metabolic consumption of oxygen in tissues: the weakly diamagnetic oxyhemoglobin releases strongly paramagnetic O_2 and deoxyhemoglobin molecules (71). The magnetic susceptibility χ remained very stable, with only a minimal increase at arrival of 1.75 ± 0.43 versus 1.49 ± 0.34 ppm at baseline (Supplemental Digital Content 8, values of urinary and blood biomarkers at four time points, http://links.lww.com/MSS/C181), as expected in low-intensity aerobic exercise where the average intensity remains less than 50% of $\dot{V}O_{2max}$ (57), explaining the lack of significant variations over time. Indeed, measurable changes in magnetic susceptibility-related measures in skeletal muscles reported in the literature occurred only in critical conditions such as cuff compression tests or ischemia (72). Our differences among muscle heads and groups are, however, in line with findings by others (72). This finding is explained by the differences among muscles in slow-twitch oxidative muscle fibers, different capillary density, and myoglobin content.

From a broader perspective, the proposed approach could also serve in diseases for longitudinal monitoring of muscular disorder progression or improvement due to various treatments. Indeed, the motivation for both athletes and physicians during this study was also to serve and encourage technological developments that could, beyond a deeper understanding of muscle physiology during extreme exercise, also help, in turn, be a crucial adjunct to improve patient diagnosis, follow-up, and care and evaluate the effects of personalized-designed therapies, a highly critical objective not in clinical routine. Indeed, there are several clinical scenarios in which pathologies lead to inflammation or muscle wasting. Moreover, such an approach could be coupled to the other strengths of MRI, including *in vivo* dynamic imaging of muscle function and kinematics (73–76), muscle microstructure using diffusion MRI or measures of chemical changes associated with metabolic states, and glycogen consumption using MR spectroscopy (77).

Limitations. Although we have studied the average response for all the subjects, there is an interindividual response heterogeneity that is likely influenced by factors such as age (78), training status (79), performance level, experience, and many others that likely modulated the inflammatory response but could not be taken into account because of our limited sample size.

In this article, we used simple statistical descriptors to analyze the quantitative indexes extracted at each time point and within each muscle head, whereas radiomic features could have been explored for each quantitative index.

Although considering the results on PDFF, it should be kept in mind that the PDFF values in our study are especially low because our subjects are professional athletes and there are estimation errors in PDFF map computation.

Recently, more specific acquisition methods and modeling, combining ultrashort echo time acquisition (9) and muscle-specific models of diffusion, might enable short-term distinguishing the T2 of each muscle compartment (T2 intracellular, T2 in the membrane, T2 extracellular) and thus elucidating the different causes of changes in the parameters.

CONCLUSIONS

Using a model of prolonged and extreme mechanical stress, we showed that a dedicated analysis pipeline enables the extraction of local quantitative imaging markers of inflammation and metabolic response and the detection of local changes related to exercise. Our study confirms that prolonged MUMs induce singular muscle damages compared with other sporting events, whereas the extreme eccentric load (due to the 24,000 m

of downhill running) is likely the main trigger. When applied with proposed segmentation and analysis pipeline, qMRI can monitor these changes while differentiating the involvement of the heads of the quadriceps muscle.

There are many potential applications; for example, in sports science, our approach could be used to explore the effect of other exercise challenges or to quantify the effects of training strategies or training programs on specific individuals. Considering that MRI can also provide high-spatial-resolution anatomical images of muscle injuries and trauma, as well as information on muscle microstructure and metabolic variables such as glycogen consumption, qMRI would be a highly relevant noninvasive modality for investigating the relationship among force loss, muscle microstructure, performance and recovery in athletes, and muscle wasting and disability in patients.

This work was performed within the framework of the LABEX PRIMES (ANR-11-LABX-0063) of Université de Lyon, within the program "Investissements d'Avenir" (ANR-11-IDEX-0007) operated by the French National Research Agency (ANR). The authors thanks warmly all ultra-trailers that volunteered for the MUST project, the VDA trailers and Courmayeur city representatives for their technical assistance. The authors would also like to thank Siemens Healthcare and Carestream. The authors are especially grateful to Bavo von Riet (Siemens Healthcare Belgium) for his efficient help in setting up the whole project, Nicolas Hermann for his kindness, availability and technical assistance, Bernard Borloz and Jan Philipp Gelzer (Siemens HealthCare Switzerland), and Serge Ripart (Siemens HealthCare France) for the technical assistance and their help in upgrading the equipment of the mobile MR with state-of-the-art sequences, coils, and prototypes. The authors also thank Sysmex for their support and for providing a pocH-100i TM automated hematology analyzer (Sysmex, Villepinte, France).

The authors declare that there is no conflict of interest. The results of the present study do not constitute endorsement by the American College of Sports Medicine and are presented clearly, honestly, and without fabrication, falsification, or inappropriate data manipulation.

REFERENCES

1. Millet GP, Millet GY. Ultramarathon is an outstanding model for the study of adaptive responses to extreme load and stress. *BMC Med*. 2012;10(1):77.
2. Andonian P, Viallon M, Le Goff C, et al. Shear-wave elastography assessments of quadriceps stiffness changes prior to, during and after prolonged exercise: a longitudinal study during an extreme mountain ultra-marathon. *PLoS One*. 2016;11(11):1–21.
3. Zanchi D, Viallon M, Le Goff C, et al. Extreme mountain ultra-marathon leads to acute but transient increase in cerebral water diffusivity and plasma biomarkers levels changes. *Front Physiol*. 2017;7:664.
4. Belli T, Macedo DV, De Araújo GG, et al. Mountain ultramarathon induces early increases of muscle damage, inflammation, and risk for acute renal injury. *Front Physiol*. 2018;9:1368.
5. Saugy J, Place N, Millet GY, Degache F, Schena F, Millet GP. Alterations of neuromuscular function after the world's most challenging mountain ultra-marathon. *PLoS One*. 2013;8(6):e65596.
6. Clarkson PM, Hubal MJ. Exercise-induced muscle damage in humans. *Am J Phys Med Rehabil*. 2002;81(11 Supp):S52–69.
7. Guilhem G, Cornu C, Maffiuletti NA, Guével A. Neuromuscular adaptations to isoload versus isokinetic eccentric resistance training. *Med Sci Sports Exerc*. 2013;45(2):326–35.
8. Brown RW, Cheng YCN, Haacke EM, Thompson MR, Venkatesan R. *Magnetic Resonance Imaging: Physical Principles and Sequence Design*. 2nd ed. New York (NY): John Wiley & Sons; 2014.
9. Saab G, Thompson RT, Marsh GD. Multicomponent T2 relaxation of in vivo skeletal muscle. *Magn Reson Med*. 1999;42:150–7.
10. Ababneh ZQ, Ababneh R, Maier SE, et al. On the correlation between T(2) and tissue diffusion coefficients in exercised muscle: quantitative measurements at 3T within the tibialis anterior. *MAGMA*. 2008;21:273–8.
11. Ploutz-Snyder LL, Nyren S, Cooper TG, Potchen EJ, Meyer RA. Different effects of exercise and edema on T2 relaxation in skeletal muscle. *Magn Reson Med*. 1997;37:676–82.
12. Ran J, Ji S, Morelli JN, Wu G, Li X. T2 mapping in dermatomyositis/polymyositis and correlation with clinical parameters. *Clin Radiol*. 2018;73(12):1057.e13–1057.e8.
13. Maillard SM, Jones R, Owens C, et al. Quantitative assessment of MRI T2 relaxation time of thigh muscles in juvenile dermatomyositis. *Rheumatology*. 2004;43(5):603–8.
14. Thuny F, Lairez O, Roubille F, et al. Post-conditioning reduces infarct size and edema in patients with ST-segment elevation myocardial infarction. *J Am Coll Cardiol*. 2012;59(24):2175–81.
15. Biglands JD, Grainger AJ, Robinson P, et al. MRI in acute muscle tears in athletes: can quantitative T2 and DTI predict return to play better than visual assessment? *Eur Radiol*. 2020;30:6603–13.
16. Welsch GH, Hennig FF, Krinner S, Trattnig S. T2 and T2* mapping. *Curr Radiol Rep*. 2014;2:60.
17. Froeling M, Oudeman J, Strijkers GJ, et al. Muscle changes detected with diffusion-tensor imaging after long-distance running. *Radiology*. 2015;274(2):548–62.
18. Maeo S, Ando Y, Kanehisa H, Kawakami Y. Localization of damage in the human leg muscles induced by downhill running. *Sci Rep*. 2017;7(1):5769.
19. Leporq B, Le Troter A, Le Fur Y, et al. Combined quantification of fatty infiltration, T1-relaxation times and T2*-relaxation times in normal-appearing skeletal muscle of controls and dystrophic patients. *MAGMA*. 2017;30(4):407–15.
20. Leporq B, Ratiney H, Pilleul F, Beuf O. Liver fat volume fraction quantification with fat and water T1 and T2*estimation and accounting for NMR multiple components in patients with chronic liver disease at 1.5 and 3.0 T. *Eur Radiol*. 2013;23(8):2175–86.
21. Tawara N, Nitta O, Kuruma H, Niitsu M, Itoh A. T2 mapping of muscle activity using ultrafast imaging. *Magn Reson Med Sci*. 2011;10(2):85–91.
22. Patten C, Meyer RA, Fleckenstein JL. T2 mapping of muscle. *Semin Musculoskelet Radiol*. 2003;7(4):297–305.
23. Kikinis R, Pieper SD, Vosburgh KG. 3D slicer: a platform for subject-specific image analysis, visualization, and clinical support. In: Jolesz FA, editor. *Intraoperative Imaging and Image-Guided Therapy [Internet]*. New York (NY): Springer New York; 2014. pp. 277–89. Available from: https://doi.org/10.1007/978-1-4614-7657-3_19.
24. Gilles B, De Bourguignon C, Croisille P, Millet G, Beuf O, Viallon M. Automatic segmentation for volume quantification of quadriceps muscle head: a longitudinal study in athletes enrolled in extreme mountain ultra-marathon. In: *ISMRM2016: International Society for Magnetic Resonance in Medicine*. Singapore; 2016.
25. Bakdash JZ, Marusich LR. Repeated measures correlation. *Front Psychol*. 2017;42(2):261–7.
26. Fernandez NF, Gundersen GW, Rahman A, et al. Clustergrammer, a web-based heatmap visualization and analysis tool for high-dimensional biological data. *Sci Data*. 2017;4:170151.
27. Lucas SJE, Helge JW, Schütz UHW, Goldman RF, Cotter JD. Moving in extreme environments: extreme loading; carriage versus distance. *Extrem Physiol Med*. 2016;5:6.
28. Schütz UHW, Billich C, König K, et al. Characteristics, changes and influence of body composition during a 4486 km transcontinental ultramarathon: results from the transeurope footrace mobile whole body MRI-project. *BMC Med*. 2013;11(1):122.
29. Theysohn JM, Kraff O, Maderwald S, et al. MRI of the ankle joint in healthy non-athletes and in marathon runners: image quality issues at 7.0 T compared to 1.5 T. *Skeletal Radiol*. 2013;42(2):261–7.

30. Fulford J, Eston RG, Rowlands AV, Davies RC. Assessment of magnetic resonance techniques to measure muscle damage 24 h after eccentric exercise. *Scand J Med Sci Sport*. 2014;25(1):e28–39.
31. Fleckenstein JL. Muscle water shifts, volume changes, and proton T2 relaxation times after exercise. *J Appl Physiol*. 1993;74(4): 2047–8.
32. Fleckenstein JL, Watumull D, McIntire DD, Bertocci LA, Chason DP, Peshock RM. Muscle proton T2 relaxation times and work during repetitive maximal voluntary exercise. *J Appl Physiol (1985)*. 1993;74(6):2855–9.
33. Le Rumeur E, Carre F, Bernard AM, Bansard JY, Rochcongar P, De Certaines JD. Multiparametric classification of muscle T1 and T2 relaxation times determined by magnetic resonance imaging. The effects of dynamic exercise in trained and untrained subjects. *Br J Radiol*. 1994;67(794):150–6.
34. Skenderi KP, Kavouras SA, Anastasiou CA, Yiannakouris N, Matalas AL. Exertional rhabdomyolysis during a 246-km continuous running race. *Med Sci Sports Exerc*. 2006;38(6):1054–7.
35. Fridén J, Lieber RL. Eccentric exercise-induced injuries to contractile and cytoskeletal muscle fibre components. *Acta Physiol Scand*. 2001; 171(2):321–6.
36. Robach P, Boisson RC, Vincent L, et al. Hemolysis induced by an extreme mountain ultra-marathon is not associated with a decrease in total red blood cell volume. *Scand J Med Sci Sport*. 2014;24(1): 18–27.
37. Overgaard K, Lindstrom T, Ingemann-Hansen T, Clausen T. Membrane leakage and increased content of Na+–K+ pumps and Ca2+ in human muscle after a 100-km run. *J Appl Physiol*. 2002;92(5): 1891–8.
38. McCarthy DA, Dale MM. The leucocytosis of exercise. A review and model. *Sports Med*. 1988;6(6):333–63.
39. Hikida RS, Staron RS, Hagerman FC, Sherman WM, Costill DL. Muscle fiber necrosis associated with human marathon runners. *J Neurol Sci*. 1983;59(2):185–203.
40. Knechtle B, Duff B, Schulze I, Kohler G. A multi-stage ultra-endurance run over 1,200 km leads to a continuous accumulation of total body water. *J Sports Sci Med*. 2008;7(3):357–64.
41. Sloniger MA, Cureton KJ, Prior BM, Evans EM. Lower extremity muscle activation during horizontal and uphill running. *J Appl Physiol (1985)*. 1997;83(6):2073–9.
42. Degache F, Morin JB, Oehen L, et al. Running mechanics during the world's most challenging mountain ultramarathon. *Int J Sports Physiol Perform*. 2016;11(5):608–14.
43. Gottschall JS, Kram R. Ground reaction forces during downhill and uphill running. *J Biomech*. 2005;38(3):445–52.
44. Van Oorschot JWM, Gho JMIH, Van Hout GPJ, et al. Endogenous contrast MRI of cardiac fibrosis: beyond late gadolinium enhancement. *J Magn Reson Imaging*. 2015;41(5):1181–9.
45. Van Nierop BJ, Bax NAM, Nelissen JL, et al. Assessment of myocardial fibrosis in mice using a T2*-weighted 3D radial magnetic resonance imaging sequence. *PLoS One*. 2015;10(6):e0129899.
46. Huang SY, Li XH, Huang L, et al. T2* Mapping to characterize intestinal fibrosis in crohn's disease. *J Magn Reson Imaging*. 2018;48(3): 829–36.
47. Zia MI, Ghugre NR, Connelly KA, et al. Characterizing myocardial edema and hemorrhage using quantitative T2 and T2* mapping at multiple time intervals post ST-segment elevation myocardial infarction. *Circ Cardiovasc Imaging*. 2012;5(5):566–72.
48. Messroghli DR, Moon JC, Ferreira VM, et al. Clinical recommendations for cardiovascular magnetic resonance mapping of T1, T2, T2 and extracellular volume: a consensus statement by the Society for Cardiovascular Magnetic Resonance (SCMR) endorsed by the European Association for Cardiovascular Imaging. *J Cardiovasc Magn Reson*. 2017;19(1):75.
49. Manka R, Paetsch I, Schnackenburg B, Gebker R, Fleck E, Jahnke C. BOLD cardiovascular magnetic resonance at 3.0 Tesla in myocardial ischemia. *J Cardiovasc Magn Reson*. 2010;12(1):54.
50. Jahnke C, Gebker R, Manka R, Schnackenburg B, Fleck E, Paetsch I. Navigator-gated 3D blood oxygen leveldependent CMR at 3.0-T for detection of stress-induced myocardial ischemic reactions. *JACC Cardiovasc Imaging*. 2010;3(4):375–84.
51. Aguor EN, Arslan F, Van De Kolk CW, et al. Quantitative T2* assessment of acute and chronic myocardial ischemia/reperfusion injury in mice. *MAGMA*. 2012;25(5):369–79.
52. Lira FS, Yamashita AS, Uchida MC, et al. Low and moderate, rather than high intensity strength exercise induces benefit regarding plasma lipid profile. *Diabetol Metab Syndr*. 2010;3:31.
53. Belton PS, Jackson RR, Packer KJ. Pulsed NMR Studies of water in striated muscle. I. Transverse nuclear spin relaxation times and freezing effects. *Biochim Biophys Acta*. 1972;286(1):16–25.
54. Nemeth A, Segrestin B, Leporq B, et al. Comparison of MRI-derived vs. traditional estimations of fatty acid composition from MR spectroscopy signals. *NMR Biomed*. 2018;31(9):e3991.
55. Achten J, Gleeson M, Jeukendrup AE. Determination of the exercise intensity that elicits maximal fat oxidation. *Med Sci Sports Exerc*. 2002;42(4):405–12.
56. Jeukendrup AE, Saris WH, Wagenmakers AJ. Fat metabolism during exercise: a review—part II: regulation of metabolism and the effects of training. *Int J Sports Med*. 1998;19(5):203–302.
57. Maufrais C, Millet GP, Schuster I, Rupp T, Nottin S. Progressive and biphasic cardiac responses during extreme mountain ultramarathon. *Am J Physiol Heart Circ Physiol*. 2016;310(10):H1340–8.
58. Spriet LL. Regulation of skeletal muscle fat oxidation during exercise in humans. *Med Sci Sports Exerc*. 2002;34(9):1477–84.
59. Watt MJ, Cheng Y. Triglyceride metabolism in exercising muscle. *Biochim Biophys Acta Mol Cell Biol Lipids*. 2017;1862(10 Pt B): 1250–9.
60. Van Loon LJC. Use of intramuscular triacylglycerol as a substrate source during exercise in humans. *J Appl Physiol*. 2004;97(4): 1170–87.
61. Stankiewicz-Choroszucha B, Górski J. Effect of decreased availability of substrates on intramuscular triglyceride utilization during exercise. *Eur J Appl Physiol Occup Physiol*. 1978;40(1):27–35.
62. Kiens B, Essen-Gustavsson B, Christensen NJ, Saltin B. Skeletal muscle substrate utilization during submaximal exercise in man: effect of endurance training. *J Physiol*. 1993;469:459–78.
63. Guo Z, Burguera B, Jensen MD. Kinetics of intramuscular triglyceride fatty acids in exercising humans. *J Appl Physiol*. 2000;89(5): 2057–64.
64. Krssak M, Petersen KF, Bergeron R, et al. Intramuscular glycogen and intramyocellular lipid utilization during prolonged exercise and recovery in man: a 13C and 1H nuclear magnetic resonance spectroscopy study. *J Clin Endocrinol Metab*. 2000;85(2):748–54.
65. Décombaz J, Schmitt B, Ith M, et al. Postexercise fat intake repletes intramyocellular lipids but no faster in trained than in sedentary subjects. *Am J Physiol Regul Integr Comp Physiol*. 2001;281(3):R760–9.
66. Watt MJ, Heigenhauser GJF, Spriet LL. Intramuscular triacylglycerol utilization in human skeletal muscle during exercise: is there a controversy? *J Appl Physiol*. 2002;93(4):1185–95.
67. Kiens B, Roepstorff C, Glatz JFC, et al. Lipid-binding proteins and lipoprotein lipase activity in human skeletal muscle: influence of physical activity and gender. *J Appl Physiol*. 2004;97(4):1209–18.
68. Ferguson MA, Alderson NL, Trost SG, Essig DA, Burke JR, Durstine JL. Effects of four different single exercise sessions on lipids, lipoproteins, and lipoprotein lipase. *J Appl Physiol*. 1998;85(3):1169–74.
69. Frias MA, Virzi J, Golaz O, Gencer B, Mach F, Vuilleumier N. Impact of long distance rowing on biological health: a pilot study. *Clin Biochem*. 2018;52:142–7.
70. Schenck JF. The role of magnetic susceptibility in magnetic resonance imaging: MRI magnetic compatibility of the first and second kinds. *Med Phys*. 1996;23(6):815–50.
71. Wang Y, Liu T. Quantitative susceptibility mapping (QSM): decoding MRI data for a tissue magnetic biomarker. *Magn Reson Med*. 2015;73(1):82–101.

72. Wang C, Zhang R, Zhang X, et al. Noninvasive measurement of lower extremity muscle oxygen extraction fraction under cuff compression paradigm. *J Magn Reson Imaging*. 2016;43(5):1148–58.
73. Drace JE, Pelc NJ. Measurement of skeletal muscle motion in vivo with phase-contrast MR imaging. *J Magn Reson Imaging*. 1994;4(2): 157–63.
74. Pappas GP, Asakawa DS, Delp SL, Zajac FE, Drace JE. Nonuniform shortening in the biceps brachii during elbow flexion. *J Appl Physiol*. 2002;92(6):2381–9.
75. Asakawa DS, Blemker SS, Gold GE, Delp SL. In vivo motion of the rectus femoris muscle after tendon transfer surgery. *J Biomech*. 2002; 35(8):1029–37.
76. Zhong X, Epstein FH, Spottiswoode BS, Helm PA, Blemker SS. Imaging two-dimensional displacements and strains in skeletal muscle during joint motion by cine DENSE MR. *J Biomech*. 2008;41(3):532–40.
77. Kent-Braun JA, McCully KK, Chance B. Metabolic effects of training in humans: a 31P-MRS study. *J Appl Physiol (1985)*. 1990;69(3):1165–70.
78. Manfredi TG, Fielding RA, O'Reilly KP, Meredith CN, Lee HY, Evans WJ. Plasma creatine kinase activity and exercise-induced muscle damage in older men. *Med Sci Sports Exerc*. 1991;23(9):1028–34.
79. Newton MJ, Morgan GT, Sacco P, Chapman DW, Nosaka K. Comparison of responses to strenuous eccentric exercise of the elbow flexors between resistance-trained and untrained men. *J Strength Cond Res*. 2008;22(2):597–607.